

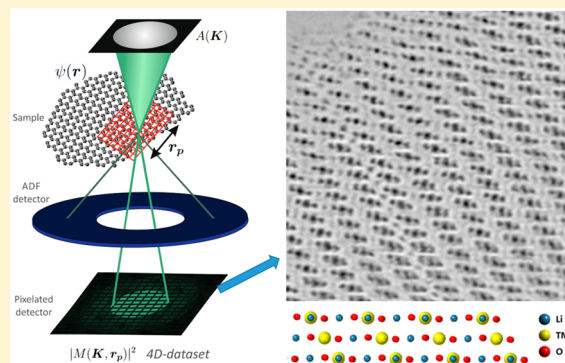
Low-Dose Aberration-Free Imaging of Li-Rich Cathode Materials at Various States of Charge Using Electron Ptychography

Juan G. Lozano,* Gerardo T. Martinez, Liyu Jin, Peter D. Nellist, and Peter G. Bruce

Department of Materials, University of Oxford, Parks Road, OX1 3PH Oxford, United Kingdom

ABSTRACT: Imaging the complete atomic structure of materials, including light elements, with minimal beam-induced damage of the sample is a long-standing challenge in electron microscopy. Annular bright-field scanning transmission electron microscopy is often used to image elements with low atomic numbers, but due to its low efficiency and high sensitivity to precise imaging parameters it comes at the price of potentially significant beam damage. In this paper, we show that electron ptychography is a powerful technique to retrieve reconstructed phase images that provide the full structure of beam-sensitive materials containing light and heavy elements. Due to its much higher efficiency, we can reduce the beam currents used down to the subpicoampere range. Electron ptychography also allows residual lens aberrations to be corrected at the postprocessing stage, which avoids the need for fine-tuning of the probe that would result in further beam damage and provides aberration-free reconstructed phase images. We have used electron ptychography to obtain structural information from aberration-free reconstructed phase images in the technologically relevant lithium-rich transition metal oxides at different states of charge. We can unambiguously determine the position of the lithium and oxygen atomic columns while amorphization of the surface, formation of beam-induced surface reconstruction layers, or migration of transition metals to the alkali layers are drastically reduced.

KEYWORDS: Electron ptychography, STEM, Li-rich cathodes, batteries, dose, beam damage



High-resolution electron microscopy is one of the most important techniques for atomic-scale characterization of the structure of materials but like all techniques suffers limitations. Two important limitations are the challenge of imaging light elements when close to heavier ones, and the structural changes that can be caused by the electron beam irradiation. In many materials, such as the Li-rich battery cathode materials addressed here, both these problems occur, light elements often being susceptible to beam damage.^{1,2} Here, we show that the emerging technique of electron ptychography can mitigate both these problems, demonstrated through imaging of Li and O in Li-rich battery cathode material while showing a reduction in beam damage. The approach is widely applicable for structural determination in materials and is particularly powerful for beam-sensitive compounds containing a wide-range of atomic numbers.

Aberration-corrected scanning-transmission electron microscopy (STEM) allows imaging the structure of materials down to subangstrom resolution with chemical information. In annular dark-field STEM (ADF-STEM) images (see Figure 1 for the optical configuration), the contrast is approximately proportional to $Z^{1.7}$, where Z refers to the atomic number,³ so it is possible to investigate composition variations at the atomic scale and even single atom impurities can be identified.⁴ Furthermore, the incoherent nature of ADF-STEM images means that they can be readily interpreted to reveal the atomic configuration of materials,⁵ and ADF-STEM is now the

dominant method for atomic-resolution imaging. When heavy and light elements are present simultaneously, however, the strong signal from the heavy elements may swamp the signal from the light elements, often rendering the light elements invisible. Furthermore, the scattering by light elements to the high angles detected in ADF is weak so the imaging is inefficient and requires a substantial illuminating dose. Annular bright-field STEM (ABF-STEM) has been developed to address this point and has been successfully used to image directly light elements such as Li, O, or N^{6–8} among others. Unfortunately, ABF-STEM is a very experimentally demanding technique because it is not tolerant to residual aberrations or mistilt of the sample.⁹ Acquiring images in ABF-STEM typically requires longer preacquisition sample tilting and microscope tuning, which implies longer times of continuous irradiation of the sample (i.e., higher accumulated electron dose) and the possibility of sample damage.

Reducing the total dose of electrons used in the experiment is an obvious solution to beam damage. To achieve this, we need to (i) limit the exposure required to optimize the optical configuration for the experiment (i.e., the final correction of focus and astigmatism) and (ii) use an imaging mode that

Received: July 4, 2018

Revised: September 11, 2018

Published: September 26, 2018

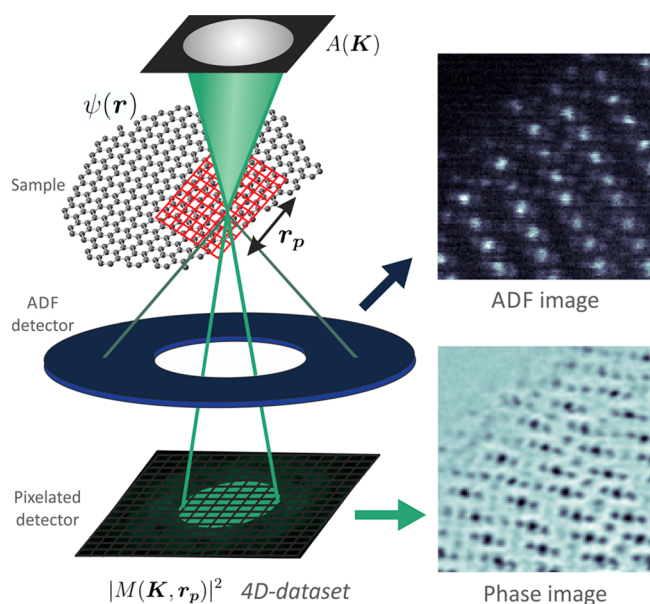


Figure 1. Schematic of 4D data set used in STEM ptychography. As the probe scans the sample, 2D information on the image plane is acquired simultaneously with 2D diffraction patterns. Therefore, each probe position in the sample plane is linked to a diffraction pattern in the diffraction plane. High-angle scattering can be simultaneously recorded by the ADF detector and the total intensity recorded by the ADF detector plotted as a function of probe position to form a simultaneous ADF-STEM image.

makes efficient use of the illuminating dose to form contrast in the image. Because of the intrinsically poor efficiency of ADF-STEM and ABF-STEM (of all the electrons that reach the detector plane, we only collect and integrate the signal over a small angular range), lowering the beam current will further worsen the signal-to-noise ratio. We therefore want a technique that is efficient in terms of use of the electron beam and is robust to small residual aberrations. It has been recently shown that electron ptychography can fulfill both of these requirements.¹⁰

The principle of electron ptychography is that a camera is used to record the intensity in the STEM detector plane for each of the different probe positions in the 2D scan, resulting in a four-dimensional (4D) data set from which phase images can be reconstructed^{11,12} (schematics shown in Figure 1). This data set consists of the full convergent beam electron diffraction pattern for each probe position that is scanned over the sample and contains all the scattering information generated by the electron-sample interaction in the STEM experiment. Ptychography can be performed with a focused or defocused probe.^{13–15} Here, we use focused probe so that the ADF-STEM signal can be also recorded simultaneously, allowing a full analysis. Electron ptychography provides phase images that have been shown to contain structural information on light elements in materials at the atomic level.¹⁰ Ptychography is well established for imaging with light and X-rays,^{16,17} but it has become feasible in the electron microscope only very recently with the advent of superfast single-electron detectors (frame speeds >1 kHz)¹⁸ and with the improvements in computing capabilities. The use of electron ptychography has three main advantages compared with the more conventionally used STEM-ADF/ABF: (i) Combined with ADF-STEM it allows heavy and light elements to be visualized

simultaneously, and experimentally it is not as demanding on precise optical alignment compared to ABF as will be shown later in this paper; (ii) it allows for postacquisition detection and correction of residual lens aberrations, avoiding the need for final focusing and stigmating which increases the specimen exposure, and optimizes the contrast in the reconstructed phase image; and (iii) much lower beam currents can be used, because effectively all the electrons that reach the detector plane are collected, as opposed to ADF- or ABF-STEM, where only a small fraction of the signal is integrated over a particular angular range. These last two advantages both make large contributions to reducing sample damage. Lowering the beam current consequently decreases the electron dose, so the beam-related fast aging of the battery is slowed down. Accurate tuning of defocus and astigmatism before image acquisition is not necessary, so we can always move across to fresh, undamaged areas of the sample, immediately record data, and then correct for aberrations at the postprocessing stage.

In this work, we have chosen lithium-rich transition metal oxide (Li-rich TMOs) cathodes as case study. We show that electron ptychography in the STEM can be used to reconstruct aberration-corrected phase images with atomic resolution in pristine, charged and discharged particles even when beam currents in the sub-pA range are used. These materials are interesting from a technological point of view since they show higher capacities and improved safety compared with the more traditional LiCoO₂, which makes them attractive for use in rechargeable Li-ion batteries.^{19–23} However, there are still several fundamental issues, most of them inherently local, that hinder their widespread implementation. These issues are related to a gradual voltage fade and irreversible capacity loss upon charge–discharge,^{24–28} which will have an effect on their electrical and ionic conductivity and on their structural integrity at the higher-scale levels. The formation of thin layers of spinel-like and rock salt phases on the surface of the cathode materials has been proposed as a possible explanation to the observed voltage fade.^{1,29–31} However, one must be extremely careful when drawing such conclusions because it has also been shown that the effect of the electron beam under some circumstances (low scan rates or continuous irradiation) can resemble the lattice reconstruction and compositional changes induced by the charge–discharge cycles.^{1,2} The use of electron ptychography would allow us to remove that uncertainty by using lower beam currents and thus reducing the beam damage. Additionally, being able to image Li and O would allow understanding important mechanisms such as degree of delithiation and Li reinsertion or changes in the O framework upon charge/discharge.

The samples consisted of Li_{1.2}Mn_{0.6}Ni_{0.2}O₂ particles fabricated by a sol–gel method.³² The experiments were carried out on an aberration-corrected JEOL ARM200F operating at 200 kV. We used a convergence angle of 22 mrad, an inner and outer collection angle of 44.4–164.5 mrad and 9.4–20.6 mrad, respectively, for the ADF and ABF detectors. In order to further minimize damage and correct for drift and scan distortions, sequences of fast ADF- and ABF-STEM images were recorded and subsequently aligned and averaged using a nonrigid registration algorithm.³³ In particular, all ABF-STEM images presented here are the average of 20 images (512 × 512 pixels, 10.6 × 10.6 nm field of view) recorded with a pixel dwell-time of 4 μs (total acquisition time is 21 s). The 4D data sets were recorded using the JEOL “4D Canvas” detector containing a pnCCD

STEM camera¹⁸ running at 4000 frames per second (image size: 512×512 pixels; field of view: 10.6×10.6 nm; pixel dwell-time: 250 μ s; total acquisition time: 65.5s). The ptychographic reconstructions were performed using an in-house MATLAB code, which is adapted from the Wigner Distribution Deconvolution method.^{10,34}

In Figure 2, we show the reconstructed amplitude and phase image from ptychographic data taken with a beam current of 6

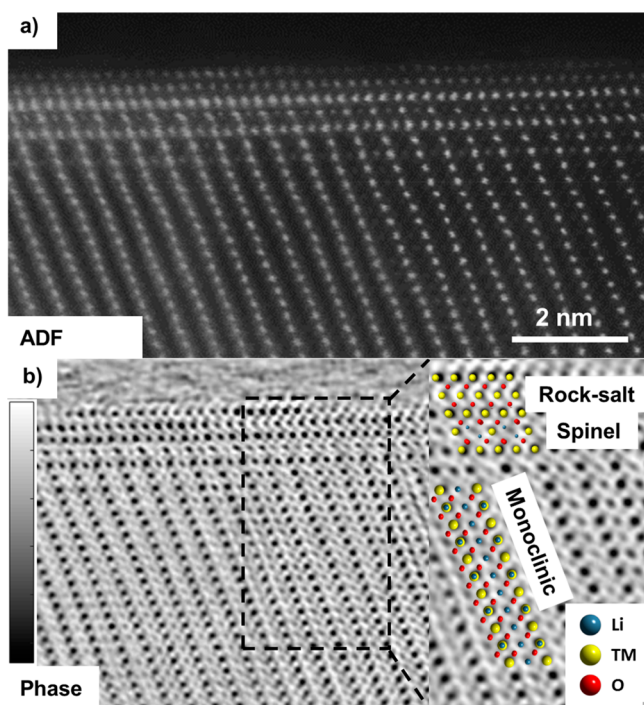


Figure 2. (a) ADF-STEM and (b) reconstructed phase image of a $\text{Li}_{1.2}\text{Mn}_{0.6}\text{Ni}_{0.2}\text{O}_2$ particle along the $[010]$ direction, which also shows a thin layer of spinel/rock-salt along the $[110]$ direction on the surface. Grayscale: 0 to -0.54 rad. The inset in (b) shows a magnified area with an atomic model superimposed indicating the positions of the transition metals (TMs), oxygen, and lithium columns.

pA of a $\text{Li}_{1.2}\text{Mn}_{0.6}\text{Ni}_{0.2}\text{O}_2$ particle along the $[010]$ direction. The observed structure agrees well with the reported monoclinic $C2/m$ layered structure throughout the particle except for a thin (<2 nm) spinel/rock-salt layer on certain facets³⁵ with orientation relationship $[010]_M \parallel [110]_{S/R-S}$, $(001)_M \parallel (1\bar{1}1)_{S/R-S}$. The oxygen atoms can also be seen in octahedral coordination around the transition metals in the reconstructed phase image, as well as certain contrast in the alkali layer. However, it is unclear at this stage whether this contrast arises from the presence of Li in the alkali layer. The reason for this is as follows: if we consider the experimental conditions used, we can estimate a depth of field under optimized imaging conditions of $\Delta z \sim 9.4$ nm.³⁶ This implies that although subangstrom resolution can be achieved laterally the final projected structure in the images is an average over a significantly larger Δz in depth. Thus, the thin layer of native spinel/rock-salt on the surface of the pristine particle will have a significant influence on the final image contrast. The contribution of this spinel/rock-salt phase will be larger at the edge of the particles and slowly decreases toward the thicker regions, where the bulk structure will dominate. For the typical thicknesses near the edge of the particles where the data are recorded, the final image will always be a superposition of

the phases (spinel/rock-salt and monoclinic). For this reason, we cannot state that the contrast observed in the alkali layers is unambiguously due to the presence of Li, because the contribution to the image contrast from the surface spinel/rock-salt phase has to be also considered.

Therefore, in order to test the potential of electron ptychography to image Li we need to remove this ambiguity by choosing different structures or orientations that allow us to image pure Li atomic columns. This is achievable if we consider the spinel/rock-salt structure along the $[110]$ orientation. As mentioned before, it is known that thin layers of spinel/rock-salt phase can be formed on the surface of the Li-rich TMOs particles upon a charge/discharge cycle. Here, the particles were charged up to 4.55 V and then discharged in order to induce the monoclinic to spinel/rock-salt transformation. By doing this we obtain areas on the surface of the particle where only the spinel/rock-salt phases are observed, with no contribution from the bulk layered structure. An example is shown in Figure 3a, where an ADF-STEM image of

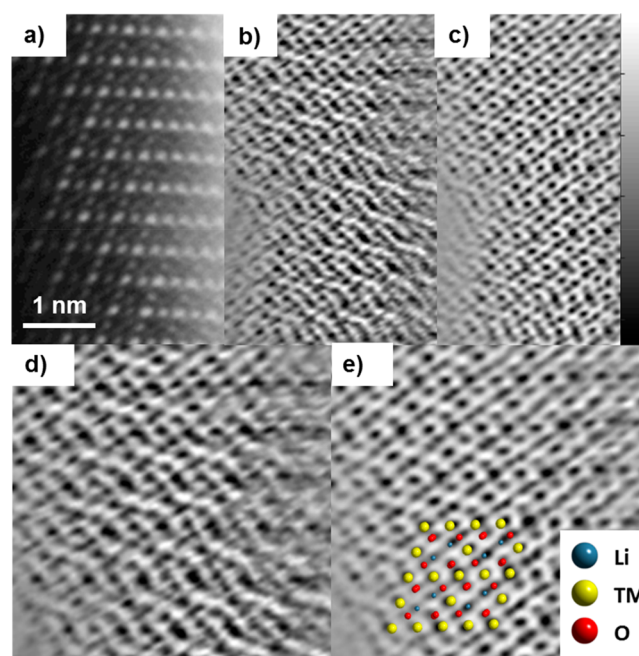


Figure 3. (a) ADF-STEM image of a thin flake of spinel phase along the $[110]$ direction near the edge of a $\text{Li}_{1.2}\text{Mn}_{0.6}\text{Ni}_{0.2}\text{O}_2$ discharged particle. The reconstructed phase images are shown in (b) before aberration correction (grayscale, 0 to -0.57 rad) and (c) after aberration correction (grayscale, 0 to -0.92 rad). (d,e) Magnified region near the edge of the flake before and after aberration correction, respectively. An atomic model is also overlaid on (e).

a thin flake of spinel/rock-salt along the $[110]$ direction at the edge of a discharged particle is displayed (beam current of 6 pA). In Figure 3b, we present the reconstructed phase image of an adjacent area, and in Figure 3d an enlarged area near the edge of the flake. When compared with the atomic model, image dips are observed in the atomic positions that would correspond to the reinserted Li. However, the close proximity of these Li columns to the neighboring oxygen columns (the Li–O distance in this projection is ~ 1.1 Å) and the presence of residual aberrations do not allow the Li columns to be clearly resolved. One of the important advantages that electron ptychography offers is the possibility of correcting the

aberrations at the postprocessing stage. For this, the probe aberrations are estimated from the same 4D data set used to retrieve the phase image, as explained in detail in ref 10. A singular value decomposition algorithm is implemented to estimate the probe aberrations from the double-overlap regions of the aperture that are observed in the 4D data set when a Fourier transform with respect to probe position is applied. After determining the probe aberration coefficients, the Wigner deconvolution process accounts for this estimated probe, leading to an aberration-free phase image. The aberration-corrected phase image of the same data set displayed in Figure 3b is now displayed in Figure 3c with the corresponding enlarged area near the edge of the flake on Figure 3e. Although before aberration-correction the Li–O pairs in the [110] projection appeared as diffuse streaks, the quality of the reconstruction improves significantly after the removal of aberrations, and the Li–O pairs are seen as well resolved dumbbells in the phase image.

So far, we have shown that it is possible to use electron ptychography to obtain full structural information in pristine and discharged samples from aberration-free reconstructed phase images. However, the main challenge is still imaging charged particles where beam damage is more significant than in pristine or discharged since after Li removal the stability of the structure decreases. In the following section, we explore the possibility of using lower beam currents to image $\text{Li}_{1.2}\text{Mn}_{0.6}\text{Ni}_{0.2}\text{O}_2$ particles charged up to 4.55 V. Table 1

Table 1. Summary of the Experimental Conditions Used in the Different Beam Currents Experiments Shown in Figure 4

emission current (μA)	beam current (pA)	total dose (e^-/nm^2)	
		ABF	ptychography
15	6	6.8×10^6	2.4×10^7
5	2	2.3×10^6	7.2×10^6
1	0.4	4.6×10^5	1.5×10^6

summarizes the microscope gun emission current, beam current, and total accumulated dose for the different conditions used in the experiment. In all cases, ABF-STEM images and ptychography data sets were recorded in fresh, adjacent areas along the edge of the same particle so we can directly compare the output of the two techniques for similar thicknesses. It should be noted that the difference in total dose between ABF-STEM and ptychography arises from the difference in the pixel dwell-time used.

Figure 4a shows the ABF-STEM (left) and ptychography reconstructed phase image (right) taken on a charged $\text{Li}_{1.2}\text{Mn}_{0.6}\text{Ni}_{0.2}\text{O}_2$ particle along the [010] direction using a beam current of 6 pA, the same used for the pristine and discharged case. Both images contain the same structural information, revealing the position of the transition metals, the oxygen atoms in octahedral coordination around them, and the contrast in the alkali layer due to the presence of a reconstructed surface. The beam current was then lowered to 2 pA (electron dose three times lower), and the results are shown in Figure 4b. While the phase image shows again the full structural information, the signal-to-noise ratio of the ABF-STEM image has decreased and now the oxygen columns are not visible. It is unclear whether the latter issue is due to the lower beam current used or to the presence of a small mistilt of the sample as we moved along the edge of the nanoparticle. In

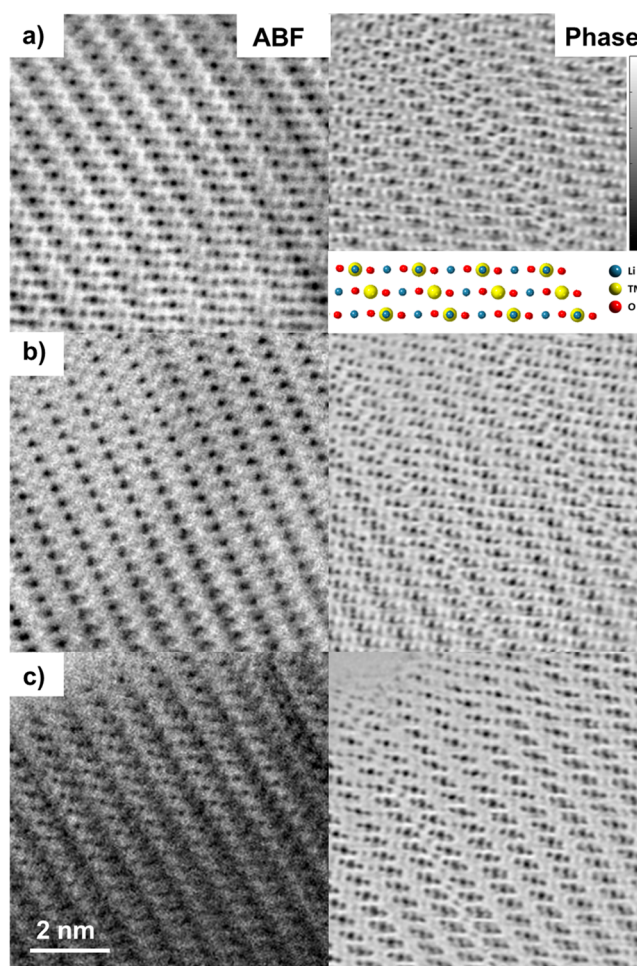


Figure 4. ABF-STEM micrographs (left) and reconstructed phase image (right) of a charged $\text{Li}_{1.2}\text{Mn}_{0.6}\text{Ni}_{0.2}\text{O}_2$ particle along the [010] direction taken with beam currents of (a) 6, (b) 2, and (c) 0.4 pA. Grayscale: (a) 0 to -0.98 , (b) 0 to -1.48 , and (c) 0 to -1.70 rad.

either case, this shows that electron ptychography is a much more robust technique, not only to aberrations as shown before, but also to mistilts that, even small, are large enough to induce loss of information in ABF-STEM. The beam current was then lowered further down to 0.4 pA see Figure 4c. For this beam current, the signal-to-noise ratio in the ABF-STEM image is too poor to reveal any structural information, while the reconstructed phase image contains the same information as for the higher beam current.

The remaining question is whether there is a significant decrease in beam damage in these materials by lowering the beam current. Figure 5 shows a region in the edge of a particle where beam damage was deliberately induced using a high electron dose ($>2.6 \times 10^8 \text{ e}^-/\text{nm}^2$). As can be seen by comparing the ADF-STEM images in Figure 5 before (left) and after (center) irradiation, using this high current results in sputtering of materials from the surface and a significant surface reconstruction. The phase image in Figure 5 (right) shows an amorphized surface, and several artifacts in the most damaged areas of the particle. However, the phase image that corresponds to the lowest beam current of 0.4 pA (Figure 4c) shows a very clean edge and no artifacts or beam-induced surface reconstruction, and even nonperiodic features such as stacking faults can be seen. Only a very thin layer at the edge of the particle that seems amorphous is observable. We cannot be

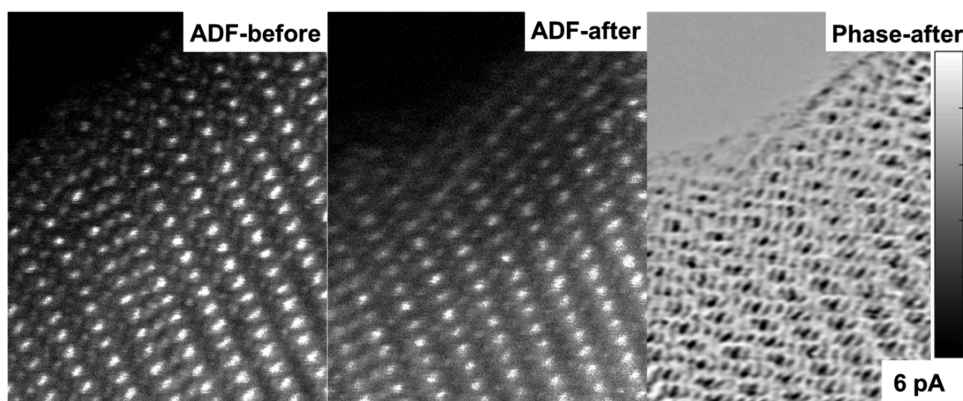


Figure 5. Beam-induced damage. The image shows an ADF-STEM image before (left), after (center), and reconstructed phase image after long irradiation using a beam current of 6 pA. Grayscale: 0 to -1.33 rad.

certain that it is not beam induced or its presence is due to different reasons. In any case, the thickness of such a layer is less than 2 Å thick, much smaller than the thicker spinel/rock-salt reported for beam damage. Remarkably, no contrast is observed in some areas of the alkali layers as would be expected in a delithiated particle. This could indicate that no rock-salt/spinel surface reconstructed layer is being formed upon irradiation at such small currents allowing the delithiation to be directly observed, as opposed to the situation for higher or intermediate beam currents (Figure 4a,b) where the formation of the rock-salt/spinel surface may preclude observation of the delithiation. Some other areas in the alkali layer show a weak contrast, which could be due to partial delithiation or to the migration of transition metals.

In conclusion, we have shown that electron ptychography in the STEM is a powerful technique to image the structure—including the light elements—of beam sensitive materials at the atomic level. Because of its high efficiency, we can use much lower currents than those used in ADF- or ABF-STEM, which drastically minimizes beam damage. Additionally, lens aberrations can be corrected in the postprocessing stage, which can be used to reduce the accumulated electron dose even further by avoiding the need for electron exposure for final optical adjustment. We have successfully used this technique to image the structure of Li-rich TMO cathode materials in the pristine, charged, and discharged state. The position of both Li and O atomic columns can be unambiguously determined. We have also shown that by using beam currents in the sub-pA range, beam-induced structural rearrangements such as amorphization or the formation of a surface reconstructed layer can be minimized. This is extremely important to avoid misinterpretation of results because we can separate beam-induced structural arrangements from those produced by the charge/discharge cycles of the material.

AUTHOR INFORMATION

Corresponding Author

*E-mail: juan.lozano@materials.ox.ac.uk

ORCID

Juan G. Lozano: 0000-0003-2900-3902

Liyu Jin: 0000-0003-1003-0855

Author Contributions

J.G.L. and G.T.M. contributed equally. J.G.L. wrote the manuscript with contributions of all authors. J.G.L., G.T.M., P.D.N., and P.G.B. designed the study. J.G.L. and G.T.M.

performed the STEM experiment. G.T.M. applied the WDD ptychography reconstruction method, and L.J. designed and synthesized the Li-rich TMOs specimens. All authors have given approval to the final version of the manuscript.

Notes

The authors declare no competing financial interest.

Supporting research data has been deposited in the Oxford Research Archive and is available under this DOI: [10.5287/bodleian:NGAON0gkG].

ACKNOWLEDGMENTS

Support from the EPSRC (EP/K040375/1 “South of England Analytical Electron Microscope”) and from Grants EP/M010708/1 and EP/K032518/1 is gratefully acknowledged. The support of JEOL Ltd (Y. Kondo and R. Sagawa) and PNDetector (M. Simson, M. Huth, and H. Soltau) is also gratefully acknowledged. P.G.B. is indebted to the EPSRC, including Enabling Next Generation Lithium Batteries EP/M00952/1 for financial support.

ABBREVIATIONS

TM(O), transition metal (oxide); STEM, scanning-transmission electron microscopy; ABF, annular bright field; ADF, annular dark field.

REFERENCES

- (1) Lu, P.; Yan, P.; Romero, E.; Spoerke, E. D.; Zhang, J.-G.; Wang, C.-M. *Chem. Mater.* **2015**, *27*, 1375–1380.
- (2) Lin, F.; Markus, I. M.; Doeff, M. M.; Xin, H. L. L. *Sci. Rep.* **2015**, *4*, 5694.
- (3) Pennycook, S. J.; Nellist, P. D. *Scanning transmission electron microscopy: imaging and analysis*; Springer Science+Business Media: New York, 2011.
- (4) Krivanek, O. L.; Chisholm, M. F.; Nicolosi, V.; Pennycook, T. J.; Corbin, G. J.; Dellby, N.; Murfitt, M. F.; Own, C. S.; Szilagy, Z. S.; Oxley, M. P.; Pantelides, S. T.; Pennycook, S. J. *Nature* **2010**, *464*, 571–574.
- (5) Nellist, P. D. *Scanning Transmission Electron Microscopy*. In *Science of Microscopy*; Hawkes, P. W., Spence, J. C. H., Eds.; Springer: New York, 2007; pp 65–132.
- (6) Findlay, S. D.; Shibata, N.; Sawada, H.; Okunishi, E.; Kondo, Y.; Yamamoto, T.; Ikuhara, Y. *Appl. Phys. Lett.* **2009**, *95*, 191913.
- (7) Okunishi, E.; Ishikawa, I.; Sawada, H.; Hosokawa, F.; Hori, M.; Kondo, Y. *Microsc. Microanal.* **2009**, *15*, 164–165.
- (8) Gu, L.; Zhu, C. B.; Li, H.; Yu, Y.; Li, C. L.; Tsukimoto, S.; Maier, J.; Ikuhara, Y. *J. Am. Chem. Soc.* **2011**, *133*, 4661–4663.

- (9) Zhou, D.; Muller-Caspary, K.; Sigle, W.; Krause, F. F.; Rosenauer, A.; van Aken, P. A. *Ultramicroscopy* **2016**, *160*, 110–117.
- (10) Yang, H.; Rutte, R. N.; Jones, L.; Simson, M.; Sagawa, R.; Ryll, H.; Huth, M.; Pennycook, T. J.; Green, M. L.; Soltau, H.; Kondo, Y.; Davis, B. G.; Nellist, P. D. *Nat. Commun.* **2016**, *7*, 12532.
- (11) Pennycook, T. J.; Lupini, A. R.; Yang, H.; Murfitt, M. F.; Jones, L.; Nellist, P. D. *Ultramicroscopy* **2015**, *151*, 160–167.
- (12) Yang, H.; Pennycook, T. J.; Nellist, P. D. *Ultramicroscopy* **2015**, *151*, 232–239.
- (13) D'Alfonso, A. J.; Allen, L. J.; Sawada, H.; Kirkland, A. I. *J. Appl. Phys.* **2016**, *119*, 054302.
- (14) D'Alfonso, A. J.; Morgan, A. J.; Yan, A. W. C.; Wang, P.; Sawada, H.; Kirkland, A. I.; Allen, L. J. *Phys. Rev. B: Condens. Matter Mater. Phys.* **2014**, *89*, 064101.
- (15) Wang, P.; Zhang, F.; Gao, S.; Zhang, M.; Kirkland, A. I. *Sci. Rep.* **2017**, *7*, 2857.
- (16) Maiden, A. M.; Morrison, G. R.; Kaulich, B.; Gianoncelli, A.; Rodenburg, J. M. *Nat. Commun.* **2013**, *4*, 1669.
- (17) Maiden, A. M.; Rodenburg, J. M.; Humphry, M. J. *Opt. Lett.* **2010**, *35*, 2585–2587.
- (18) Ryll, H.; Simson, M.; Hartmann, R.; Holl, P.; Huth, M.; Ihle, S.; Kondo, Y.; Kotula, P.; Liebel, A.; Muller-Caspary, K.; Rosenauer, A.; Sagawa, R.; Schmidt, J.; Soltau, H.; Struder, L. *J. Instrum.* **2016**, *11*, P04006.
- (19) Thackeray, M. M.; Kang, S. H.; Johnson, C. S.; Vaughey, J. T.; Benedek, R.; Hackney, S. A. *J. Mater. Chem.* **2007**, *17*, 3112–3125.
- (20) Choi, N. S.; Chen, Z. H.; Freunberger, S. A.; Ji, X. L.; Sun, Y. K.; Amine, K.; Yushin, G.; Nazar, L. F.; Cho, J.; Bruce, P. G. *Angew. Chem., Int. Ed.* **2012**, *51*, 9994–10024.
- (21) Wen, J. G.; Bareno, J.; Lei, C. H.; Kang, S. H.; Balasubramanian, M.; Petrov, I.; Abraham, D. P. *Solid State Ionics* **2011**, *182*, 98–107.
- (22) Zheng, J.; Gu, M.; Genc, A.; Xiao, J.; Xu, P.; Chen, X.; Zhu, Z.; Zhao, W.; Pullan, L.; Wang, C.; Zhang, J. G. *Nano Lett.* **2014**, *14*, 2628–2635.
- (23) Yu, X. Q.; Lyu, Y. C.; Gu, L.; Wu, H. M.; Bak, S. M.; Zhou, Y. N.; Amine, K.; Ehrlich, S. N.; Li, H.; Nam, K. W.; Yang, X. Q. *Adv. Energy Mater.* **2014**, *4*, 1300950.
- (24) Croy, J. R.; Kim, D.; Balasubramanian, M.; Gallagher, K.; Kang, S. H.; Thackeray, M. M. *J. Electrochem. Soc.* **2012**, *159*, A781–A790.
- (25) Boulineau, A.; Simonin, L.; Colin, J.-F.; Canévet, E.; Daniel, L.; Patoux, S. *Chem. Mater.* **2012**, *24*, 3558–3566.
- (26) Xu, B.; Fell, C. R.; Chi, M.; Meng, Y. S. *Energy Environ. Sci.* **2011**, *4*, 2223.
- (27) Mohanty, D.; Kalnaus, S.; Meisner, R. A.; Rhodes, K. J.; Li, J. L.; Payzant, E. A.; Wood, D. L.; Daniel, C. J. *Power Sources* **2013**, *229*, 239–248.
- (28) Yu, H. J.; Zhou, H. S. *J. Phys. Chem. Lett.* **2013**, *4*, 1268–1280.
- (29) Gu, M.; Genc, A.; Belharouak, I.; Wang, D.; Amine, K.; Thevuthasan, S.; Baer, D. R.; Zhang, J.-G.; Browning, N. D.; Liu, J.; Wang, C. *Chem. Mater.* **2013**, *25*, 2319–2326.
- (30) Zheng, J.; Xu, P.; Gu, M.; Xiao, J.; Browning, N. D.; Yan, P.; Wang, C.; Zhang, J.-G. *Chem. Mater.* **2015**, *27*, 1381–1390.
- (31) Lin, F.; Markus, I. M.; Nordlund, D.; Weng, T. C.; Asta, M. D.; Xin, H. L.; Doeff, M. M. *Nat. Commun.* **2014**, *5*, 3529.
- (32) Shaju, K. M.; Bruce, P. G. *Adv. Mater.* **2006**, *18* (17), 2330–2336.
- (33) Jones, L.; Yang, H.; Pennycook, T. J.; Marshall, M. S. J.; Van Aert, S.; Browning, N. D.; Castell, M. R.; Nellist, P. D. *Advanced Structural and Chemical Imaging* **2015**, *1*, 8.
- (34) Rodenburg, J. M.; Bates, R. H. T.; et al. *Philos. Trans. R. Soc. London A* **1992**, *339*, 521–553.
- (35) Shukla, A. K.; Ramasse, Q. M.; Ophus, C.; Duncan, H.; Hage, F.; Chen, G. *Nat. Commun.* **2015**, *6*, 8711.
- (36) Cosgriff, E. C.; Nellist, P. D. *Ultramicroscopy* **2007**, *107*, 626–634.